Check for updates

Earth's Future

RESEARCH ARTICLE
10.1029/2021EF002052

Special Section:
The Arctic: An AGU Joint Special Collection

Vatnajökull Mass Loss Under Solar Geoengineering Due to the North Atlantic Meridional Overturning Circulation

Chao Yue[1], Louise Steffensen Schmidt[2], Liyun Zhao[1,3], Michael Wolovick[1], and John C. Moore[1,4,5]

[1]College of Global Change and Earth System Science, Beijing Normal University, Beijing, China, [2]Department of Geosciences, University of Oslo, Oslo, Norway, [3]Southern Marine Science and Engineering Guangdong Laboratory, Zhuhai, China, [4]CAS Center for Excellence in Tibetan Plateau Earth Sciences, Beijing, China, [5]Arctic Centre, University of Lapland, Rovaniemi, Finland

Abstract The objective of solar geoengineering by stratospheric aerosol injection (SAI) is to lower global temperatures, but it may also have adverse side effects. Iceland is situated close to the overturning regions of the Atlantic Meridional Overturning Circulation (AMOC) that warms the North Atlantic area. Hence, this may be one region where reduced irradiance by SAI may not be successful in reducing impacts from greenhouse gas warming. We examine this proposition by estimating how the Icelandic Vatnajökull ice cap (VIC) surface mass balance (SMB) and surface runoff changes in response to greenhouse gas and solar geoengineering scenarios over the period 1982–2089. We use the surface energy and mass balance model SEMIC driven by Earth System Model output under the GeoMIP G4, and CMIP RCP4.5 and RCP8.5 greenhouse gas scenarios. Geoengineering significantly reduces VIC near-surface air temperature by 0.4°C, downward longwave radiation by 2.4 Wm^{-2} and increases snowfall by 4.9 mm yr^{-1} relative to RCP4.5. During the SAI period 2020–2069, modeled annual mean SMB under G4, RCP4.5 and RCP8.5 are -0.34 ± 0.18 m yr^{-1}, -0.56 ± 0.06 m yr^{-1} and -0.66 ± 0.04 m yr^{-1}, respectively; surface runoff reduction under G4 is $6 \pm 6\%$ and $7 \pm 6\%$ (95% confidence interval uncertainties) compared with that under RCP4.5 and RCP8.5, which is far smaller than the $20 \pm 2\%$ and $32 \pm 2\%$ reductions for the Greenland ice sheet. The differences may be attributed to the reinvigoration of AMOC under G4 relative to RCP4.5 which brings more heat to Iceland than Greenland, leading to around half the cooling and longwave radiation reductions than for Greenland.

Plain Language Summary The unique location of Iceland, near the overturning regions of the Atlantic thermohaline overturning circulation, makes its response to climate change rather atypical. The overturning circulation supplies a lot of heat to Iceland, but this has been slowing, and is projected to reduce further as greenhouse warming continues over the century. Solar geoengineering has the potential to lower temperatures by artificially increasing planetary albedo and is predicted to reverse this decline in ocean circulation heat transport, but also reduces the direct warming effects of increasing amounts of greenhouse gases. Hence, the net effect on temperatures and the ice on Iceland is a delicate balance, which we explore by simulating the response of the largest ice cap Vatnajökull. The ice cap mass loss would indeed be slightly reduced by geoengineering (6%), but the effectiveness is much lower than for other glaciers globally where effectiveness is 20%–35%.

Key Points:
- We use bias corrected mass and energy balance modeling to estimate Vatnajökull surface mass balance under solar geoengineering
- 5 Tg yr^{-1} sulphate aerosol injection into the stratospheric may reduce Vatnajökull ice cap runoff by 6%
- Ice melt is reduced by far less than for Greenland because of proximity to the North Atlantic circulation overturning regions

Supporting Information:
Supporting Information may be found in the online version of this article.

Correspondence to:
L. Zhao and J. C. Moore,
zhaoliyun@bnu.edu.cn;
john.moore.bnu@gmail.com

Citation:
Yue, C., Schmidt, L. S., Zhao, L., Wolovick, M., & Moore, J. C. (2021). Vatnajökull mass loss under solar geoengineering due to the North Atlantic meridional overturning circulation. *Earth's Future*, *9*, e2021EF002052. https://doi.org/10.1029/2021EF002052

Received 2 MAR 2021
Accepted 25 JUL 2021

© 2021. The Authors.
This is an open access article under the terms of the Creative Commons Attribution-NonCommercial License, which permits use, distribution and reproduction in any medium, provided the original work is properly cited and is not used for commercial purposes.

1. Introduction

Icelandic glaciers are rather sensitive to climate warming (e.g., Guðmundsson et al., 2011; Schmidt et al., 2018, 2020). This is because of their extreme maritime setting giving them high snowfall, and ice temperatures that are always close to the melting point, leading to both large accumulation rates in their upper reaches and rapid melt in their ablation zones. Iceland sits at the confluence of the warm Irminger and cold East Iceland ocean currents (e.g., Ólafsson et al., 2007) leading to a temperate maritime climate (Vilhjálmsson, 2002). Iceland is situated close to the overturning regions of the Atlantic Meridional Overturning Circulation (AMOC) that brings significant heat to the North Atlantic region. Atmospheric greenhouse gas concentration increases tend to reduce AMOC, albeit with heavily model-dependent results (Caesar

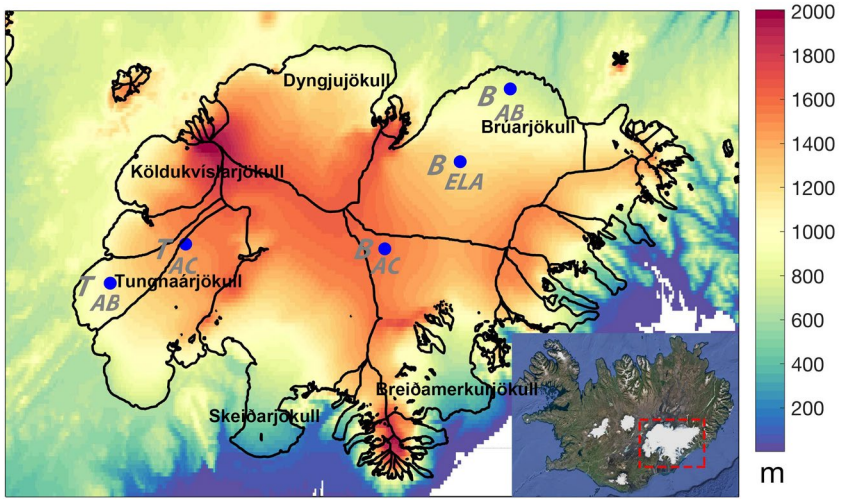

Figure 1. Surface elevation over Vatnajökull from SRTM30 and the location of the Automatic Weather Station (blue dots and gray fonts) as well as some outlet glaciers (black fonts). B_{AB} and T_{AB} are over the ablation zone, T_{AC} and B_{AC} are over the accumulation zone, B_{ELA} is near the equilibrium line altitude. Lower right corner is the view of Iceland from Google Earth, red dashed box is the Vatnajökull domain.

et al., 2018; Hong et al., 2017; Liu et al., 2017; Rahmstorf et al., 2015; Robson et al., 2014). Anthropogenic aerosol reductions also cause a slowdown in AMOC in simulations covering the time period since the 1980s (Hassan et al., 2021; Menary et al., 2020), as well as the near future (Ma et al., 2020) when aerosols are projected to decrease by the middle of the current century. Hence, for much of the North Atlantic, heat flux reduction because of AMOC slowdown offsets the increased radiative forcing due to greenhouse gases to varying degrees (potentially completely, e.g., Liu et al., 2017). The net effect in Iceland is likely to be a delicate balance between changes in irradiation and ocean heat advection.

Glaciers and ice caps in Iceland presently cover ~11% of the land surface (Björnsson & Pálsson, 2008). Changes in the fraction of snow and ice are important, as they lead to major changes in albedo. Melting all Icelandic glaciers would raise global mean sea level by only about 1 cm (Björnsson & Pálsson, 2008; Björnsson et al., 2013). This is not particularly significant relative to the much larger contributions expected from the Greenland or Antarctic ice sheets and represents only about 2% of that stored in ice caps and glaciers outside these polar ice sheets. Here, we are interested in using Iceland impacts to explore AMOC variability rather than examine Iceland's impacts on global climate. But, the changes predicted for Iceland would have large impacts locally, not only on the natural ecosystems, landscape, and hydrology, but also the psychology of Icelanders who identify themselves with the "land of ice and fire." Mass loss from Icelandic glaciers has been accelerating as a consequences of warming temperatures over recent decades (Björnsson et al., 2013) and therefore has received extensive study.

The Vatnajökull ice cap (VIC) is the largest nonpolar ice cap in Europe with an area of ~7,700 km^2 and a volume of ~2,870 km^3 (Aðalgeirsdóttir et al., 2020). VIC is near the southeastern coast of Iceland and has a maximum surface elevation of ~2,100 m above sea level (Figure 1). Mass loss from VIC has accelerated from a slightly positive mass balance in the 1980s toward a negative balance in the mid-1990s as the result of rising temperatures, possibly linked with a weakening of the North Atlantic subpolar gyre (Björnsson et al., 2013). Mass balance continued to decrease, dropping to −0.8 m yr^{-1} between 1995 and 2014 (e.g., Pálsson et al., 2015), but then it was close to zero in 2017 (Pálsson et al., 2017). There have been few studies looking at its evolution in the future, and none looking at potential geoengineering scenarios. Schmidt et al. (2020) showed that its volume will eventually decrease by 51%–94% and area by 24%–80% by the year 2300 under the representative concentration pathway (RCP) 8.5 scenario. Flowers et al. (2005) examined the sensitivity of VIC hydrology and dynamics over the next centuries. Their simulated ice cap area reduces by 12%–15% and volume by 18%–25% under 2°C warming by the end of the 21st century. Marshall et al. (2005) found that VIC volume and area are very sensitive to small temperatures shifts via simulations under various future warming rates.

Geoengineering may be broadly defined as large-scale geotechnical approaches that deliberately modify the climate system to counteract anthropogenic global warming (Shepherd, 2009). Geoengineering by stratospheric aerosol injection (SAI) has been the most thoroughly investigated methodology proposed to date. SAI potentially mimics the climate impact of large volcanic eruptions that reduce surface temperatures by scattering incoming solar radiation. About a dozen different Earth System Models (ESMs) have evaluated various SAI scenarios (Boucher et al., 2013), finding consistently that SAI reduces global temperatures in a spatially nonuniform pattern, changes precipitation patterns and lowers global mean humidity and precipitation (Kravitz et al., 2013). However, an important consideration is that SAI may also have adverse side effects that diminish or reverse the intended environmental impacts. One such adverse impact would be changes in global atmospheric or oceanic circulation that play important roles in redistributing energy around the Earth.

Of the literature discussing SAI, the most relevant here deal with its impact on the cryosphere, especially the ice sheets. Early studies considering SAI geoengineering for Greenland used a single ESM and looked at its long-term response (Applegate & Keller, 2015; Irvine et al., 2009). These studies also used simplified surface mass and energy balance parameterizations, often forced by changes in temperature and precipitation only. Ignoring changes in downward radiation flux was expected to underestimate the effectiveness of solar geoengineering at offsetting melt in Greenland (Irvine et al., 2018), and analysis from multiple ESMs showed the importance of reduced humidity reducing surface temperatures via increased long wave radiation into space (Moore et al., 2019).

However, the effectiveness of SAI relative to RCP4.5 on the mass balance of the Greenland ice sheet (Moore et al., 2019), was only about half that on glaciers in High-Mountain Asia (Zhao et al., 2017) because of the compensating changes in AMOC. Mass loss from the VIC will accelerate in the future (Schmidt et al., 2020) under greenhouse gas forcing scenarios. Whether VIC will be more or less effectively preserved by SAI than Greenland, is not obvious.

One issue in analysis of ice sheet response is the horizontal resolution of the atmospheric grids in CMIP5 ESMs (around 200 km), and even though improved under CMIP6, they are typically more than 50 km. These resolutions are coarse compared with the smaller scale (km to tens of km) of the glaciers, especially the ablation regions where melt occurs and to a large extent, the overall mass balance is shaped. We address this by using downscaling and bias correction methods that take the ESM climate fields and modify them according to high-resolution surface topography, along with in situ and satellite observations of albedo and glacier mass balance. There are advantages in this methodology for Iceland and VIC in particular, which has been well studied for many decades with a wealth of meteorological and glaciological observations (e.g., Aðalgeirsdóttir et al., 2020; Jóhannesson et al., 2020).

In this study, we choose the GeoMIP G4 scenario to explore the effect of SAI because it has been performed by several ESMs allowing across-model comparison. The G4 scenario specifies injection of sulfate aerosols into the equatorial lower stratosphere in addition to the RCP4.5 emissions scenario. We also simulate the VIC response under the RCP4.5 scenario as a direct control, and the more extreme high emissions RCP8.5 scenario which provide for a larger signal-to-noise ratio. We want to answer these questions: How does VIC quantitatively respond under the RCP4.5, RCP8.5, and SAI G4 scenarios? Could SAI mitigate VIC ice loss due to global warming? How different are the Greenland ice sheet and VIC responses, and how important is the AMOC response to Arctic ice masses?

2. Methodology

2.1. Climate Forcing and Statistical Downscaling

2.1.1. Climate Forcing

We simulate VIC SMB and surface runoff under climate projections from four ESMs (Table 1). These are the only ESMs that simulated both the GeoMIP (Geoengineering Model Intercomparison Project) G4 and CMIP5 (Coupled Model Intercomparison Project Phase 5) RCP4.5 and RCP8.5 scenarios, and have daily forcing fields as input for SEMIC (Table 2). GeoMIP has developed new experiments for use with CMIP6 level ESMs (Kravitz et al., 2015.), but yet there are relatively few models with output available. Of the ESMs

Table 1
Earth System Models (ESMs) in Coupled Model Intercomparison Project Phase 5 (CMIP5) Used in This Study

Earth system model	Atmosphere	Ensemble	Reference
BNU-ESM	2.8° × 2.8°	1	Ji et al. (2014)
HadGEM2-ES	1.25° × 1.875°	3	Collins et al. (2011)
MIROC-ESM	2.8° × 2.8°	1	Watanable et al. (2011)
MIROC-ESM-CHEM	2.8° × 2.8°	3	Watanable et al. (2011)

we use, MIROC-ESM and MIROC-ESM-CHEM share most processes except for using an interactive atmospheric chemistry module in MIROC-ESM-CHEM. Moore et al., (2019) estimated the differences in the ensemble if the MIROC models were each down weighting to 0.75 of the other two models, but found it made little difference to the mass loss. In the ESM literature, the MIROC models are considered as independent and weighted equally with other ESMs, and we follow that practice here.

The RCP8.5 scenario used to be known as the "business-as-usual" scenario with a high radiative forcing at 8.5 Wm^{-2} by 2100 (Riahi et al., 2011), however the 2015 Paris Climate Accord places the National Determined Contributions (NDCs) to greenhouse gas emissions closer to the RCP4.5 scenario (Kitous & Keramidas, 2015; Thomson et al., 2011), and might be now considered as the only internationally agreed political pathway in future emissions. Although the NDCs are meant to be strengthened over time, individual states may abrogate their commitments, and so both RCP8.5 and RCP4.5 might be considered as framing an envelope of plausible emissions over the 21st century. The G4 scenario specifies 5 Tg yr^{-1} of SO_2 to be injected into the equatorial lower stratosphere during 2020–2069 simultaneous with RCP4.5 forcing (Kravitz et al., 2013). The simulation period we focus on, spans 1982–2089 and is comprised of the CMIP5 historical simulations from 1982 to 2005, continuing with the RCP scenarios to 2089. G4 branches off the RCP4.5 scenario at 2020 with 50 years of SAI followed by cessation in 2069 and 20 years of RCP4.5 forcing. The final 20 years test the termination impacts of a sudden end to SAI. G4 has of course not yet been implemented, but it is supposedly neither technologically difficult nor prohibitively expensive (Smith & Wagner, 2018). In practice, an SAI implementation would be much more sophisticated than G4, for example, aiming to preserve existing hemispheric temperature balance, as well as equator-to-pole temperature gradients (Kravitz et al., 2016), and with seasonally varying injection rates. These types of implementations might be expected to for example, well preserve Arctic sea ice (Lee et al., 2021), along with and AMOC and Greenland ice sheet mass balance (Tilmes et al., 2020). Although detailed analyses of differences between this kind of SAI deployment and the simple version applied here have not been done, they appear to be second order compared with the impacts introduced by temperature rises due to greenhouse gas scenarios.

Table 2
Input Climate Forcing for SEMIC Model

Variable	Unit
Snowfall rate	m s^{-1}
Rainfall rate	m s^{-1}
Downward shortwave radiation	Wm^{-2}
Downward longwave radiation	Wm^{-2}
Near-surface air temperature	K
Near-surface specific humidity	kg kg^{-1}
Surface wind speed	m s^{-1}
Surface pressure	Pa
Air density	kg m^{-3}

2.1.2. Bias Correction and Downscaling

We used the European Center for Medium-Range Weather Forecasts ERA5 reanalysis product (Hersbach et al., 2020) during the period of 1982–2018 to statistically bias correct the ESM output. This product has been satisfactorily evaluated for Greenland ice sheet SMB (Delhasse et al., 2020) and for the surface-layer meteorology over Iceland (Renfrew et al., 2020). As ERA5 has a relatively coarse resolution (30 km) over Vatnajökull, we first downscale it to a 0.025° × 0.025° grid to better capture the ice topography.

Over Vatnajökull (Figure S1), surface elevation is well correlated with daily mean downward longwave radiation ($LW\downarrow$; $R = 0.77$), shortwave radiation ($SW\downarrow$; $R = 0.74$), near-surface air temperature (T; $R = 0.83$), and specific humidity (Q; $R = 0.77$) during the period of 1982–2018. We therefore bilinearly interpolate these fields to 0.025° × 0.025° grids using fitted lapse rates: $LW\downarrow$ −11.9 Wm^{-2} km^{-1}, $SW\downarrow$ 15.85 Wm^{-2} km^{-1}, T

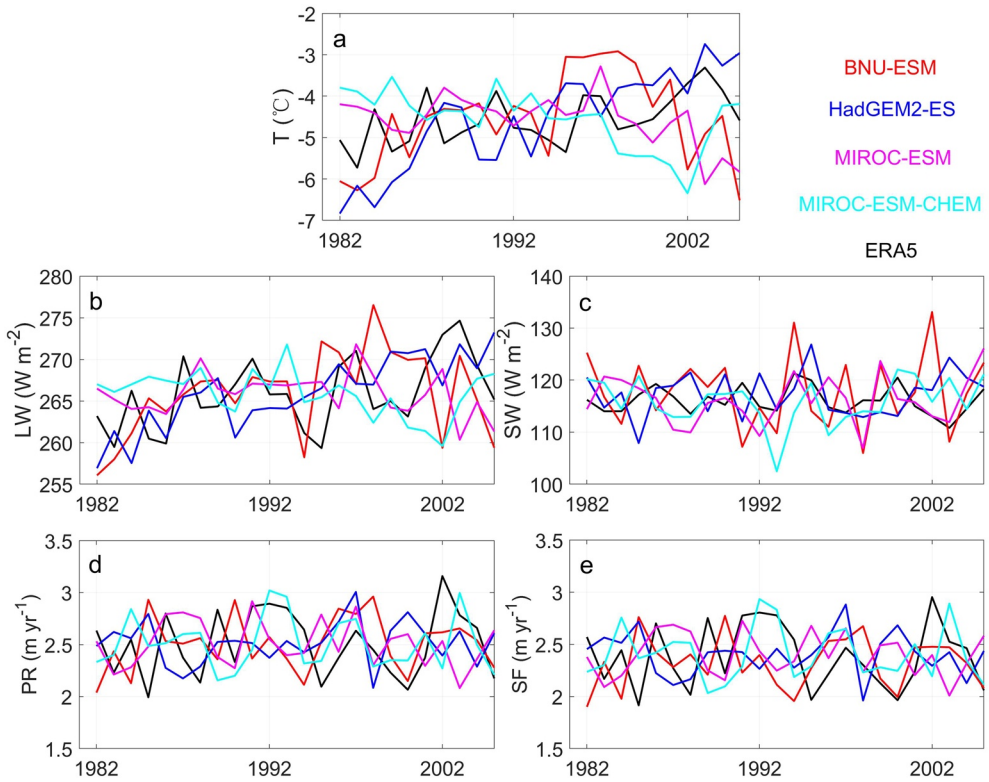

Figure 2. Historical time series of downscaled and bias-corrected (a) annual near-surface air temperature, (b) downward longwave radiation, (c) downward shortwave radiation, (d) total precipitation, and (e) snowfall by BNU-ESM (red), HadGEM2-ES (blue), MIROC-ESM (magenta), MIROC-ESM-CHEM (cyan), and downscaled ERA5 (black) during 1982–2005 over Vatnajökull.

-5.4 K km^{-1}, and Q -0.59 k k^{-1} km^{-1}. Precipitation (PR) is adequately described by an exponential relationship with surface elevation (H, unit: m) in Equation 1:

$$\mathrm{PR} = \mathrm{PR}_0 k^{H/1000} \quad (1)$$

where PR_0 is the precipitation at a reference altitude and k is a constant. Over Vatnajökull, De Ruyter-de Wildt et al. (2004) fit this equation by using the winter mass balance data during 1993–1999 and take k as 2.3. We applied this and downscaled precipitation using the Kriging interpolation method, which is suitable for smooth interpolation and has been widely used in precipitation interpolation (e.g., Bajat et al., 2013; Bostan et al., 2012; De Ruyter-de Wildt et al., 2004). The snowfall downscaling technique also follows De Ruyter-de Wildt et al. (2004), and was derived from the downscaled precipitation, assumed equal to precipitation rate when the daily mean near-surface air temperature is below 3°C. Surface wind speed, air density, and atmospheric pressure were simply bilinearly interpolated because of their minor impact on SMB in the SEMIC parameterizations.

After we downscaled ERA5, we then use it as the observation-based reference climate to downscale and bias-correct ESMs fields to the same 0.025° × 0.025° grid using the Inter-Sectoral Impact Model Intercomparison Projection (ISI-MIP; Hempel et al., 2013) method, which preserves the long-term absolute/relative trend of the simulated climate forcings. The daily variability and monthly mean of simulated climate forcing are adjusted with either a constant offset (near-surface air temperature) or multiplicative correction factor (other climate fields) calculated by the differences of simulated and observed data during the historical period. Air density is generated through the corrected near-surface air temperature and surface pressure with the ideal gas equation. We plot the five bias-corrected climate variables that are most important to SMB in comparison the downscaled ERA5 in Figure 2; bias-corrected variables share the same means and trends as their downscaled ERA5 counterparts.

2.2. The Surface Energy and Mass Balance Model, SEMIC

The SEMIC model utilizes the energy and mass balance approach to simulate the main surface processes involved in SMB, surface runoff, and snow-pack evolution. It is a model of intermediate complexity which balances the computational cost with physical parameterizations and has been shown to provide good agreement with the state-of-the art regional climate model MAR (Fettweis et al., 2013), in simulations of Greenland ice sheet surface temperature and SMB (Krapp et al., 2017), and has been used in various future projection scenarios for the ice sheet (Moore et al., 2019; Rückamp et al., 2018). It has not previously been used for Icelandic glaciers, and we did not adjust the default parameters that were tuned over Greenland. The main function of the parameters is to aid albedo parameterization, and using the Greenland parameter values produces notable differences from observed albedo over Iceland due to features that cannot be simulated with SEMIC. To correct for this deficiency, we bias-corrected the modeled albedo (Section 2.4). In all simulations, we apply a fixed ice mask that from SRTM30 digital elevation model (Farr et al., 2007), since the ice extent changes less than 10% in the dynamic simulations of Schmidt et al. (2020).

2.3. Correction of SEMIC Modeled SMB Due to SMB-Elevation Feedback

Taking account of the SMB-elevation feedback is essential for estimating future SMB and surface runoff, increased ice melt will lower the surface elevation, leading to higher temperatures and then increased melt. We took surface elevation data from the SRTM30 digital elevation model, generated from a combination of Shuttle Radar Topography Mission data and the U.S. Geological Survey's GTOPO30 data set (Farr et al., 2007). The SRTM30 has a spatial resolution of 1/120° and is designated for the year 2000; we assume it represented the whole 1982–2005 period.

We analyzed the correlation between SEMIC modeled SMB and surface elevation over the whole VIC driven by climate from each ESM during the historical period 1982–2005 (Figure S2). We found significant linear correlations ($R^2 > 0.7$; $p < 0.01$, Figure S2) between surface elevation and modeled SMB over the whole VIC during the period 1982–2005 for all the ESMs. To estimate the SMB-elevation feedback, we assumed steady state for the historical period 1982–2005, that is, surface elevation change is zero and the SMB was balanced by the divergence of the ice flux. We then assume that SMB anomalies relative to the historical averaged SMB will cause elevation change from the year 2006 onward, that is, we assume constant ice flux divergence. The cumulative SMB anomaly and SMB elevation gradient we calculated gave the correction term for SMB (Figure S3). This "historical steady state" assumption will not be fully correct since most of the outlet glaciers of Vatnajökull are surge-type glaciers that have an important effect on its volume change (Björnsson et al., 2003). A glacier undergoing a surge causes substantial anomalous mass transport from the upper accumulation zone to the ablation zones. Predicting outlet glacier surges is presently beyond even sophisticated ice dynamics models (Gong et al., 2018) and these models can only capture behavior statistically rather than predictably. However, our constant dynamics assumption still improves our estimates for surface elevation change compared with ignoring ice dynamics all together.

2.4. Surface Albedo Parameterization

Surface albedo is an important component in the calculation of surface energy balance and dominates seasonal snowmelt and surface runoff. Recent studies have shown that dust has substantial influence on the mass balance of VIC (Wittmann, et al., 2017). Local volcanic eruptions produce tephra and additional dust deposition that also lower the surface albedo (Gunnarsson et al., 2021). In the northern ablation zone of VIC, the lowest surface albedo observed by satellite imagery is less than 0.1, which was confirmed in situ (De Ruyter-de Wildt et al., 2004; Gascoin et al., 2017). Vatnajökull's albedo could not be fully described in the SEMIC albedo schemes due to the lack of dust-albedo parameterization (Figure 3). Instead, satellite observations are an efficient way to analyze VIC albedo. The GLASS (Global Land Surface Satellites) data set provides long-term continuous, gapless and self-consistent global land surface albedo product with a 0.05° × 0.05° and 8-day spatiotemporal resolution. They are generated from multisource remote sensing data with an accuracy similar to the widely acknowledged product of the Moderate Resolution Imaging Spectroradiometer (Liang et al., 2013). Compared to the Automatic Weather Stations (AWS) observations (Figure 1, Schmidt et al., 2017), the GLASS product greatly underestimates the VIC winter albedo (Figure 3).

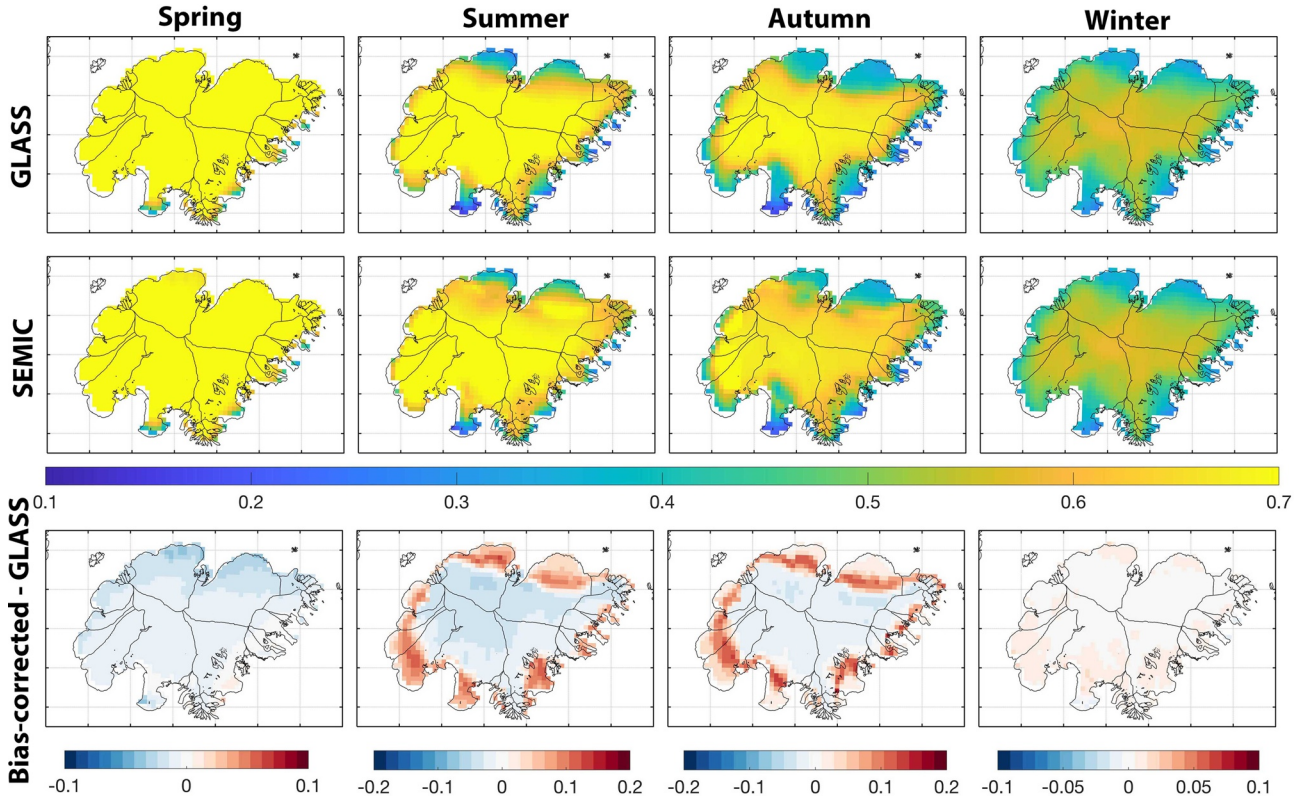

Figure 3. Spatial distribution of mean surface albedo for spring, summer, autumn, and winter during 1982–2000 from the satellite observation of Global Land Surface Satellites (GLASS) product (first row) and SEMIC outputs (second row). Bottom row is the difference: bias-corrected SEMIC output minus GLASS.

These unexpected values are caused by the decreased incoming solar irradiance and the increased solar zenith angles that effectively lower the quality of albedo retrievals (Gunnarsson et al., 2021). However, the low-biased winter albedo has very little impact on ice melt due to the low winter air temperatures; a change in winter albedo from 0.1 to 0.8 increases winter melt by <10% over the whole VIC. Therefore, we assume a winter bias has negligible effects on SMB and surface runoff, and use GLASS to bias-correct the SEMIC modeled surface albedo. Detailed albedo parameterization in SEMIC is given in Supporting Information S1. We regridded the GLASS albedo product during the period of 1982–2000 to a daily, 0.025° × 0.025° spatio-temporal resolution to be consistent with our topographic and SEMIC grids.

The procedure we followed was to first apply the SEMIC model to simulate the VIC surface albedo for all scenarios and ESMs (Section 2.1). Then, we used the regridded GLASS albedo as the observation-based reference albedo to bias-correct the modeled albedo using the ISI-MIP method (Hempel et al., 2013). The bias-corrected SEMIC and GLASS surface albedo agree well over the whole VIC ($R = 0.97$; $p < 0.01$), as is shown in Figure 3. Finally, we used bias-corrected surface albedo and ESM fields to run SEMIC to calculate the VIC SMB and surface runoff under historical, G4, RCP4.5, and RCP8.5 scenarios.

3. Results

3.1. Evaluation With Observations

To verify the performance of our bias-corrected ESM results, we compared three energy flux variables with observations from five AWS (locations see Figure 1) over VIC during the months April-October for the period 2001–2014: near-surface air temperature (T), downward shortwave radiation ($SW\downarrow$), and downward longwave radiation ($LW\downarrow$). Table 3 shows the comparison of the modeled and observed T, $SW\downarrow$, and $LW\downarrow$ during the period 2001–2014. In general, modeled $SW\downarrow$ over all stations were underestimated compared to observations by all ESMs by tens of percent (Table 3, Tables S1–S4), while modeled T and $LW\downarrow$ were

Table 3
Comparison of Downscaled and Bias-Corrected Near-Surface Air Temperature (T, °C), Downward Longwave Radiation (LW↓, Wm^{-2}) and Downward Shortwave Radiation (LW↓, Wm^{-2}) for Multimodel Mean and Observations From AWS Measurements During the Months April–October for the Period 2001–2014 (Schmidt et al., 2017)

	T (°C)		$LW\downarrow$ (Wm^{-2})		$SW\downarrow$ (Wm^{-2})	
Station	Obs.	SEMIC-Obs.	Obs.	SEMIC-Obs.	Obs.	SEMIC-Obs.
B_{AB}	274.1	0.5	290.6	−5.5	189.1	−30.3
T_{AB}	274.0	−0.2	287.3	−3.3	220.8	−60.3
T_{AC}	272.1	−0.2	274.1	5.8	247.2	−67.7
B_{AC}	271.6	−0.8	280.9	−4.3	236.8	−42.4
B_{ELA}	272.9	−0.6	283.9	−3.6	229.3	−49.9

Note. Individual model results are in Tables S1–S4.

much closer to observations. The observational uncertainties in T, $SW\downarrow$ and $LW\downarrow$ are ±0.2°C, ±10%, and ±10%, respectively (Guðmundsson et al., 2009; Kipp & Zonen, 2000).

Using the minimum and maximum relative differences between bias-corrected ESM forcing and the AWS observations for each variable, we find ranges of −0.8–0.5°C in T, −5.5–5.8 Wm^{-2} in $LW\downarrow$, and −67.7–−30.3 Wm^{-2} in $SW\downarrow$ relative to the measured values (T_0, $LW\downarrow_0$, $SW\downarrow_0$). The large differences in $SW\downarrow$ also exist in the ERA5 reanalysis as well as the bias-corrected ESMs. This is likely because $SW\downarrow$ is mainly affected by clouds and aerosols (Wild et al., 2013) that are very localized over the ice cap and which the models do not capture well. Using the SEMIC model and bias-corrected albedos, we made a sensitivity study of surface runoff to the errors in Table 3. Over the whole VIC, a 0.8°C drop in T produces a 9% runoff reduction. 67.7 Wm^{-2} and 5.5 Wm^{-2} lowerings of $SW\downarrow$ and $LW\downarrow$ reduces runoff by 19% and 10%, respectively. The uncertainty estimates in radiative flux observations are about 10%, so while these discrepancies are larger than hoped, there is little that can be done given the limitations of models. Typically, uncertainties in SMB on Icelandic ice caps (Aðalgeirsdóttir et al., 2020) and the Greenland ice sheet (Mouginot et al., 2019) are 10%. Thus, uncertainty in radiative flux makes significant, but not ruinous errors in estimates of SMB.

3.2. Downscaled and Bias-Corrected Forcing

During the SAI period 2020–2069, the ensemble-mean near-surface air temperature and downward longwave radiation under G4 is 0.4°C and 2.4 Wm^{-2} lower than that under RCP4.5 (Figure 4, Table 4), indicating the cooling effect of the G4 scenario. Global mean cooling under G4 is similar as that over VIC, but it is only half that over the Greenland ice sheet (Moore et al., 2019). However, the degree of relative cooling varies across models, with little cooling effect for two MIROC models, but 1°C and 5 Wm^{-2} and 0.7°C and 3.7 Wm^{-2} for T and $LW\downarrow$ reductions for BNU-ESM and HadGEM2-ES (Table 4). The consistency in downward shortwave radiation varies among each model, for example, it shows negative trends in all ESMs expect HadGEM2-ES; G4 significantly increases it by 3.1 Wm^{-2} in BNU-ESM, while significantly decreases by 0.4 Wm^{-2} in HadGEM2-ES and has insignificant differences in the two MIROC models (Figure 4, Table 4). As noted in Section 3.1, $SW\downarrow$ is not captured well by ESMs over polar regions, and the lack of significant change for VIC is a repeat of the situation over Greenland (Moore et al., 2019), where no models showed any difference in $SW\downarrow$ between G4 and RCP4.5. However, the notable reductions in surface temperatures attributed to reduced humidity, indicate that SAI induced changes are complex and depend on more than simple local radiative balance. The MIROC models have been seen to produce relatively small changes in many climate fields due to both greenhouse gas and SAI forcing in the polar areas (Chen et al., 2020; Moore et al., 2019). Snowfall shows decreasing trends in all scenarios for all ESMs, mainly due to increasing near-surface air temperature. However, precipitation has no significant trends in any scenarios. Precipitation under G4 is slightly higher than that under RCP4.5 in all ESMs except BNU-ESM. Spatial differences between the G4 and RCP4.5 scenarios during the SAI period 2020–2069 and post-SAI period 2075–2089 are shown in Figure 5. Perhaps surprisingly, the SAI impacts continue to hold after the termination of SAI. Based on a Wilcoxon sign-rank test with a significance level of 95% during SAI, the G4 and RCP4.5 differences in T and $LW\downarrow$ are significant over the whole VIC. There is decadal variability in the driving climate actors in Figure 4. Block et al. (2020) showed that initial conditions for Arctic sea ice and phases of the long period climate cycles driving temperature play very important roles in explaining across-ESM variability. There are large differences between the two MIROC models (Figure 4) with notably a rise in $SW\downarrow$ at 2070 not seen in MIROC-ESM-CHEM. Chen et al. (2020) suggest that similar large differences between the MIROC models in soil temperature argues that natural variability over the 50-year simulations is as large as differences due to model formulation, and hence supports the analysis of Block et al. (2020).

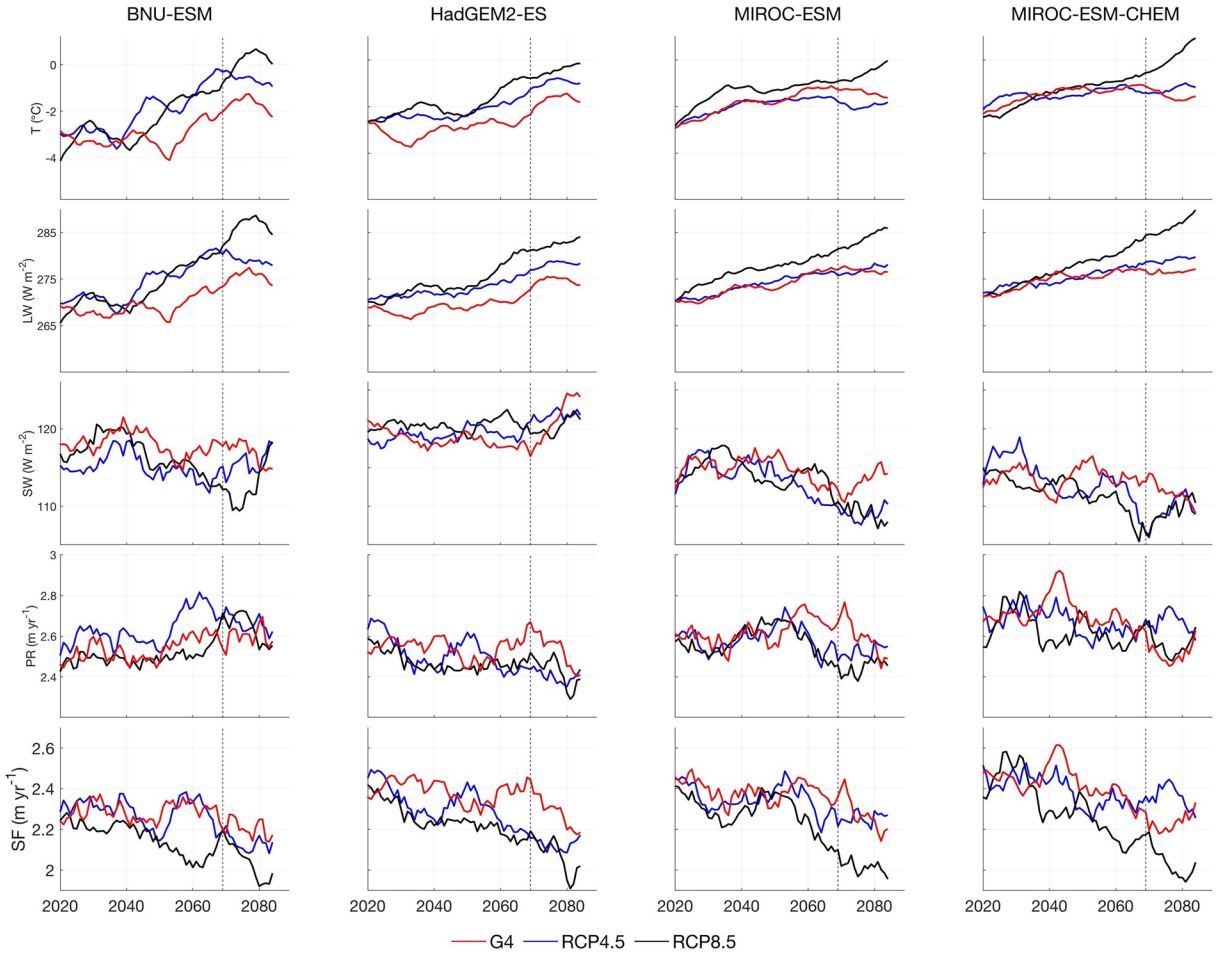

Figure 4. Decadal mean of downscaled and bias-corrected *T*, *LW*↓, *SW*↓ precipitation (PR), and snowfall (SF) during 2020–2089 over Vatnajökull ice cap (VIC), under G4 (red), RCP4.5 (blue), and RCP8.5 (black) from (left to right): BNU-Earth System Model (ESM), HadGEM2-ES, MIROC-ESM, and MIROC-ESM-CHEM. Vertical dotted lines indicate the termination of SAI geoengineering.

3.3. Surface Mass Balance and Runoff

Our simulated historical trend in SMB is similar with that found by Schmidt et al. (2020) who modeled it with the regional climate model HIRHAM5, forced with the numerical weather prediction model HARMONIE-AROME. However, our simulation generally overestimates SMB by a ~0.2 m yr^{-1} over the period 1982–

Table 4
Difference (G4-RCP4.5) Climate Forcing Over Vatnajökull Ice Cap (VIC) During Stratospheric Aerosol Injection (SAI) (2020–2069)

Model	T (°C)	LW (Wm^{-2})	SW (Wm^{-2})	PR (mm yr^{-1})	SF (mm yr^{-1})	Global T (°C)
BNU-ESM	**−1.0**	**−5.0**	**3.1**	**−9.5**	**0.8**	**−0.8**
HadGEM2-ES	**−0.7**	**−3.7**	**−0.4**	2.4	**6.6**	**−1.1**
MIROC-ESM	**0.1**	**−0.4**	1.1	4.8	5.2	**−0.4**
MIROC-ESM-CHEM	0	−0.3	0.4	3.5	3.1	**−0.3**
Ensemble	**−0.4**	**−2.4**	**1.1**	−0.2	**4.9**	**−0.6**

Note. Entries in bold are significant at the 95% level according to the Wilcoxon signed-rank test.
Abbreviation: ESM, Earth System Model; LW, longwave radiation; PR, precipitation; SF, snowfall; SW, shortwave radiation; T, Near-surface air temperature.

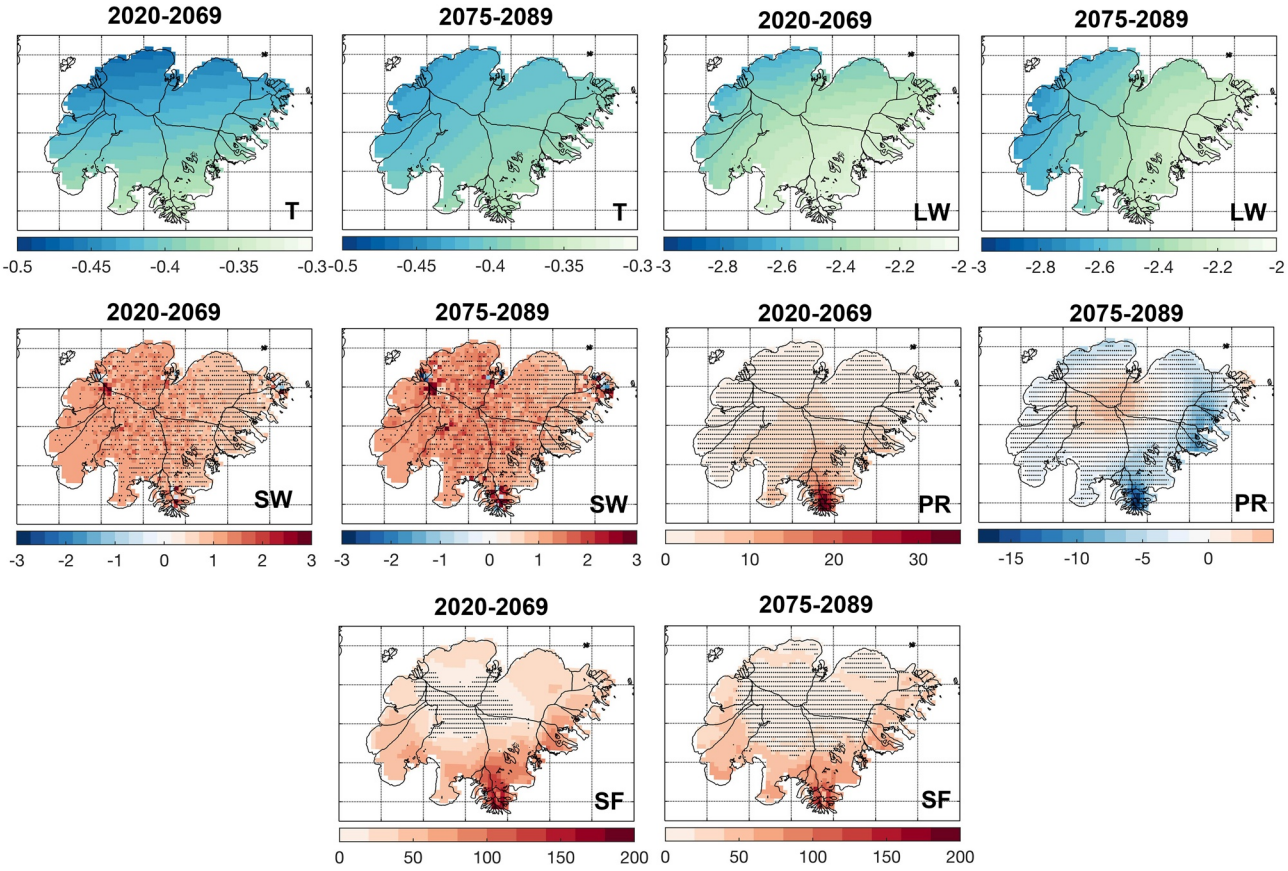

Figure 5. Earth System Model (ESM) ensemble mean spatial differences (G4-RCP4.5) in near-surface air temperature (T, °C), downward longwave radiation (LW, Wm^{-2}), downward shortwave radiation (SW, Wm^{-2}), precipitation (PR, mm yr^{-1}) and snowfall (SF, mm yr^{-1}) during stratospheric aerosol injection (SAI) 2020–2069 and after termination 2075–2089 over Vatnajökull. Stippling indicates regions where differences are not significant at the 95% level by the Wilcoxon signed-rank test. Individual model results are shown in Figures S4–S7.

2014. The modeled annual SMB averaged over the VIC is well correlated ($R = 0.6$; $p < 0.05$) with the annual in situ mass balance measurements (interpolation of on average 60 sites available for the period 1991–2010; Björnsson et al., 2013). The spatial distribution of the modeled SMB over the historical period 1980–2005 is shown in Figure 6. The accumulation zone is the high-altitude regions, especially for the southern part with surface elevations above 1,400 m (Figure 1) and SMB exceeds 8 m yr^{-1} there, while the ablation zone is over the ice cap margin where the surface albedo less than 0.5 (Figure 2). The low surface albedo leads to huge surface runoff and consequently negative SMB. Through the across-model standard deviation of SMB (Figure 6), we can conclude that individual models show relatively large differences in SMB over ablation zones, especially over Breiðamerkurjökull and eastern coast outlet glaciers, the inconsistency in ablation is mainly caused by BNU-ESM, which has distinctly lower SMB than the other three models (Figure S8). Over accumulation zones, modeled SMB are similar for all models with a standard deviation less than 0.2 m yr^{-1}. Multimodel mean SMB for 2010–2020 increases both under RCP4.5 and RCP8.5 and then subsequently decreases over 2020–2089 (Figure 7e). During the SAI period 2020–2069, all ESMs project that SMB under G4 is larger than that under RCP4.5 and RCP8.5 (Figure 7, Table 5). G4 increases annual mean SMB by 0.19 m relative to RCP4.5 and 0.3 m relative to RCP8.5, mainly because of the contributions from BNU-ESM and HadGEM2-ES because the two MIROC models exhibit little SMB differences between G4 and RCP4.5 (Figures 7c and 7d). After the termination year of 2069, the mitigating impact still holds in all ESMs.

The spatial pattern of SMB differences between G4 and RCP4.5 scenario is shown in Figure 8. Clearly, multimodel mean SMB under G4 is significantly larger than that under RCP4.5 over almost the whole VIC both during the SAI and the post-SAI period. HadGEM2-ES predicts the largest SMB increases under G4 compared with RCP4.5, up to 800 mm yr^{-1} over Tungnaárjökull. In the two MIROC models, the differences

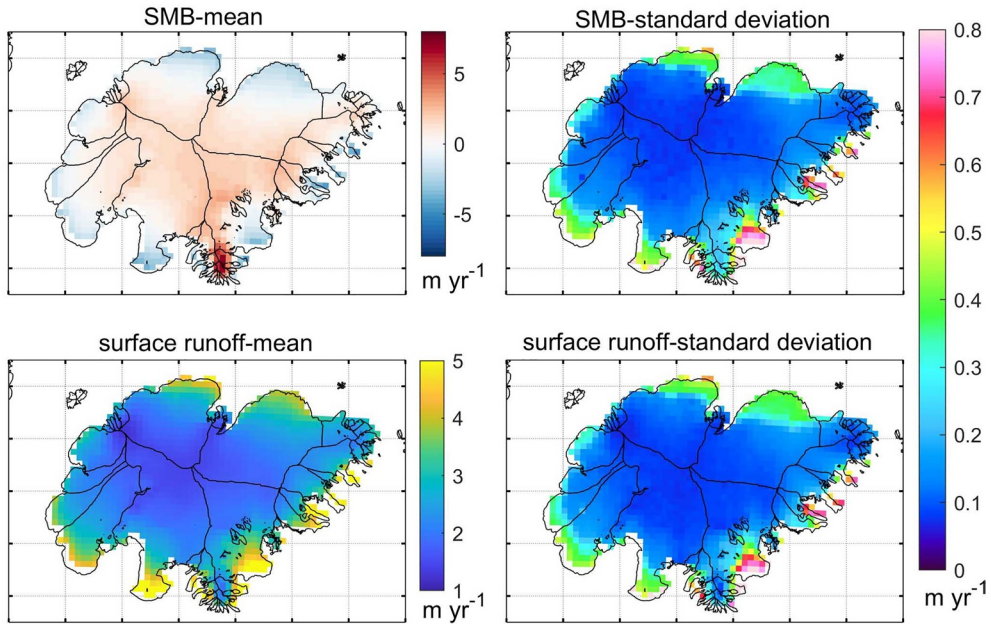

Figure 6. Spatial distribution of modeled mean surface mass balance (SMB) and surface runoff and their standard deviation during 1980–2005 from multimodel mean.

in SMB between G4 and RCP4.5 during SAI is insignificant. This is because of their small differences (G4-RCP4.5) in temperature and longwave radiation (Figure 4, Table 4) and the positive contribution of SMB from increased snowfall (although Table 4 shows this is not significant at the 95% level).

Spatio-temporal changes in surface runoff is negatively correlated with SMB (Figures 6–9). During the SAI period 2020–2069, G4 reduces runoff by 6.2 ± 6.2% (uncertainties given are 95% confidence intervals, $N = 4$), and 7.2 ± 6.0% relative to RCP4.5 and RCP8.5, respectively. By the year 2089, the SMB-elevation feedback under RCP4.5 and RCP8.5 yields 7 ± 1% and 8 ± 1% increases in runoff.

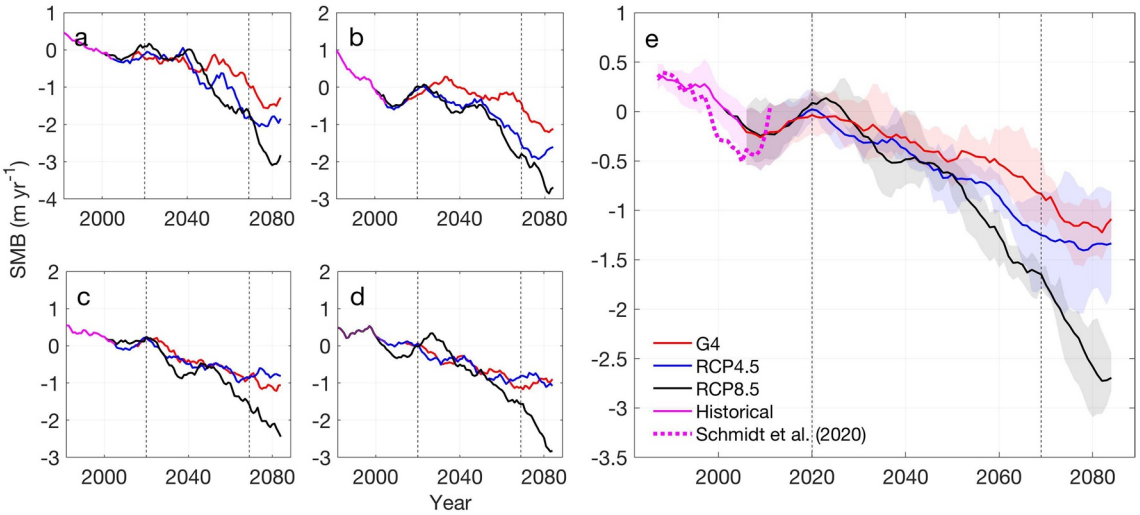

Figure 7. Decadal means of SEMIC modeled surface mass balance (SMB) averaged over the whole Vatnajökull ice cap (VIC) by BNU-Earth System Model (ESM) (a), HadGEM2-ES (b), MIROC-ESM (c), MIROC-ESM-CHEM (d), and ensemble mean (e) under historical (magenta), G4 (red), RCP4.5 (blue), and RCP8.5 (black) during 1982–2089. Dotted magenta curve is SMB during 1982–2016 from Schmidt et al. (2020) from the regional climate model HIRHAM5, forced with the numerical weather prediction model HARMONIE-AROME. Vertical dotted lines denote the start and the end of the stratospheric aerosol injection (SAI). Color shadings in (e) are the across-model spread.

Table 5
Modeled Surface Mass Balance (SMB) (m yr^{-1}) and Surface Runoff (m yr^{-1}) During the Stratospheric Aerosol Injection (SAI) Period 2020–2069 Over the Whole Vatnajökull Ice Cap (VIC) by the Four Earth System Models (ESMs) and Their Ensemble Mean Under G4, RCP4.5, and RCP8.5 Scenarios and Relative Changes Under G4 to RCP4.5 and RCP8.5 (With 95% Confidence Intervals, N = 4)

	BNU-ESM		HadGEM2-ES		MIROC-ESM		MIROC-ESM-CHEM		Ensemble	
SMB and runoff	SMB	Runoff	SMB	Runoff	SMB	Runoff	SMB	Runoff	SMB	Runoff
G4	−0.38	3.48	−0.11	3.15	−0.37	3.55	−0.55	3.76	−0.34 ± 0.18	3.46 ± 0.25
RCP4.5	−0.63	3.84	−0.52	3.56	−0.48	3.59	−0.58	3.77	−0.56 ± 0.06	3.69 ± 0.13
RCP8.5	−0.66	3.71	−0.71	3.69	−0.67	3.81	−0.60	3.75	−0.66 ± 0.04	3.73 ± 0.05
(G4-RCP4.5)/RCP4.5	--	−9.4%	--	−11.5%	--	1.1%	--	−0.3%	--	−6.2 ± 6.2%
(G4-RCP8.5)/RCP8.5	--	−6.2%	--	−14.6%	--	−6.8%	--	0.3%	--	−7.2 ± 6.0%

4. Discussion

4.1. Comparison of VIC and Greenland Ice Sheet Response to SAI

The overall analysis of SAI G4 simulations over the VIC in our study suggests that SAI would reduce surface runoff by 6.2 ± 6%. The relatively large uncertainty reflects the across model spread in results, particularly the small changes simulated by the two MIROC models (Table 4), and that we give the 95% confidence interval rather than standard error of the mean. This across-model spread of results may seem rather large, but as shown by Chen et al. (2020) and Block et al. (2020), the initial conditions of the ESMs, reflecting long period variability in sea ice and long-period climate system oscillations, means that this error estimate is indicative of lack of tuning of these initial states. Even if the ESMs were tuned via data assimilation to

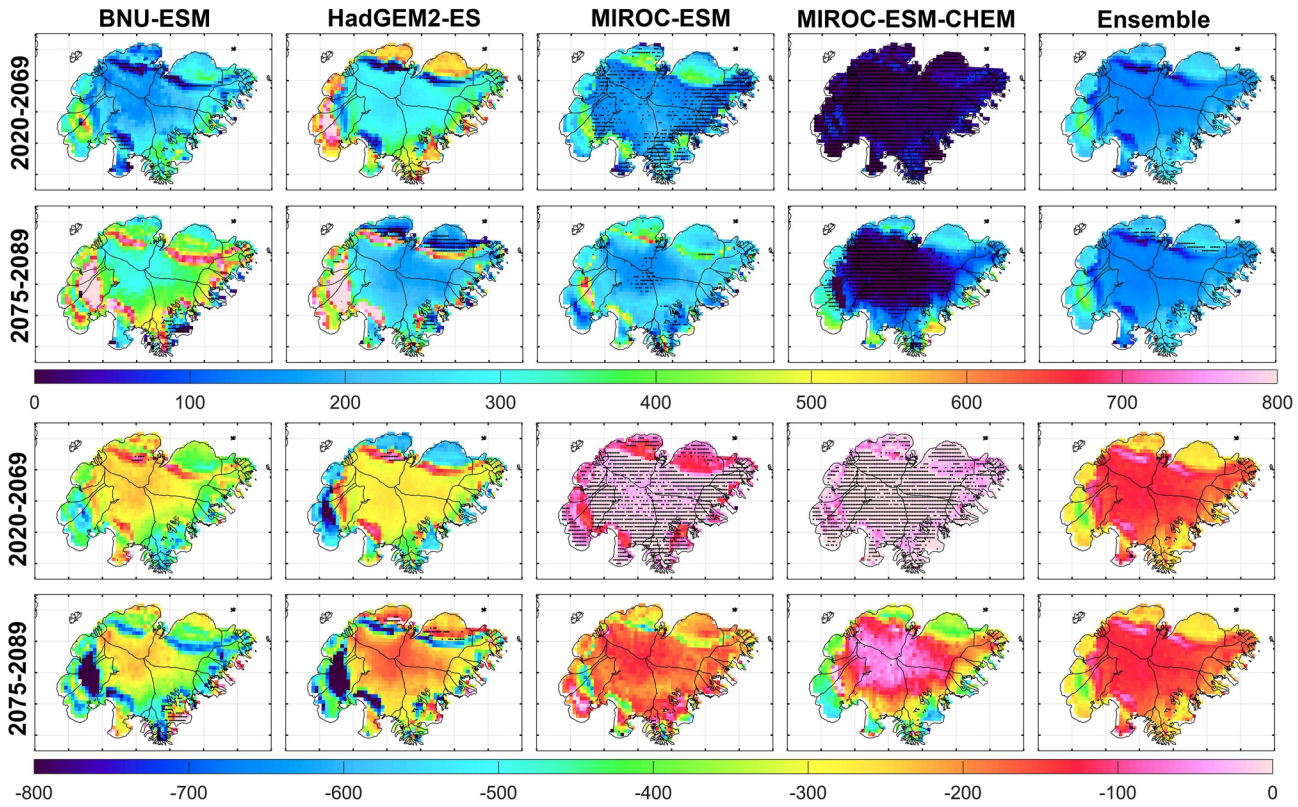

Figure 8. Spatial differences (G4-RCP4.5) of modeled surface mass balance (SMB) (top two rows, unit: mm yr^{-1}) and surface runoff (bottom two rows, unit: mm yr^{-1}) during the period 2020–2069 and 2070–2089 for the four Earth System Model (ESM) and their ensemble mean over Vatnajökull ice cap (VIC). Stippling indicates regions where differences are not significant at the 95% level by the Wilcoxon signed-rank test.

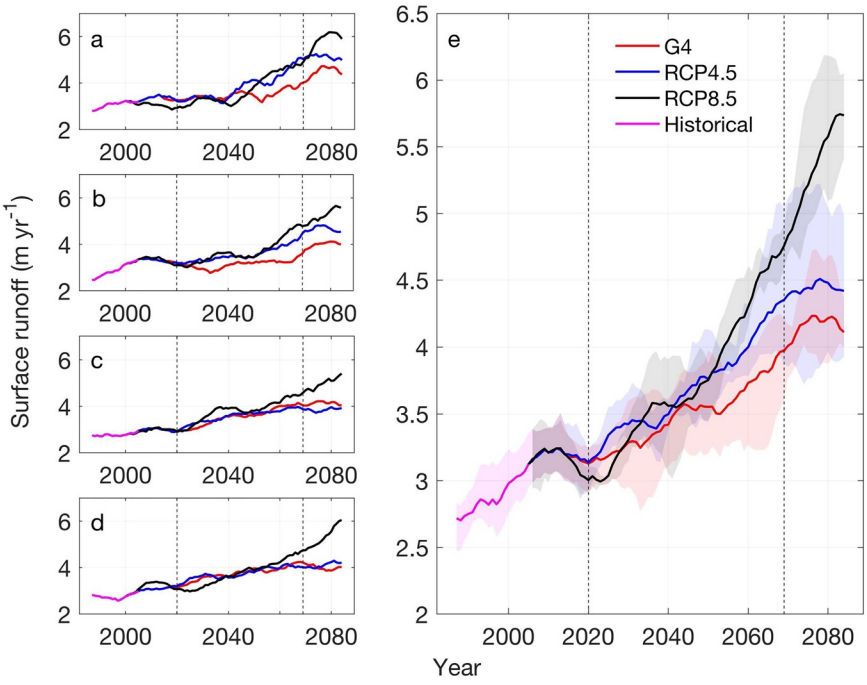

Figure 9. Decadal means of SEMIC modeled surface runoff averaged over the whole Vatnajökull ice cap (VIC) by BNU-Earth System Model (ESM) (a), HadGEM2-ES (b), MIROC-ESM (c), MIROC-ESM-CHEM (d), and ensemble mean (e) under historical (magenta), G4 (red), RCP4.5 (blue), and RCP8.5 (black) during 1982–2089. Vertical dotted lines denote the start and the end of the stratospheric aerosol injection (SAI). Color shadings in (e) are the across-model spread.

match the last decade of observations there would still be uncertainties. One reason is the less than perfect formulation of the shortwave radiative forcing, which seem to be around 20% less than observations, although these estimates of uncertainty are themselves likely to have large uncertainties of about 50% if they are Gaussian. Furthermore, it is difficult to achieve better than 10% precision in observations of surface mass balance, making SMB and runoff an elusive target.

The lowered ice wastage is through reduced near-surface air temperature and downward longwave radiation compared with greenhouse gas forcing alone. Although the SAI cooling effect is evident in our simulations, it is weaker than the 20% runoff reduction simulated over the Greenland Ice Sheet (Moore et al., 2019) and 35% reductions in High Mountain Asia (Zhao et al., 2017) by the same four ESMs as here. Relative to RCP4.5, G4 reduces surface temperatures by only 0.4°C and longwave radiation by 2.4 Wm^{-2} over VIC, which are only 36% and 52% of the reductions over Greenland. BNU-ESM projects the largest temperature and longwave radiation reductions among four ESMs both over VIC and Greenland, while HadGEM2-ES is moderate and the two MIROC models least (Figure 10). G4 significantly reduces precipitation and snowfall by −15.9 mm yr^{-1} and -5.2 mm yr^{-1} over Greenland relative to RCP4.5, but by close to zero for precipitation and produces a slight increase in snowfall over VIC. Furthermore, the differences (G4-RCP4.5) in shortwave radiation over VIC and Greenland are small and inconsistent in sign (Figure 10).

The proximate cause of these differences in response is the difference in heat flux from ocean to atmosphere under the different scenarios local to Greenland and Iceland. Figure 11 illustrates this by showing the (G4-RCP4.5) differences for the three ESMs with available data. In the grid cells surrounding the coasts of Greenland and Iceland, the heat flux is very different: for Greenland the (G4-RCP4.5) differences are (−1.2, 0, and −0.5) Wm^{-2} for BNU-ESM, MIROC-ESM, and MIROC-ESM-CHEM, respectively, while for VIC they are (8, 7.9, and 15.6) Wm^{-2}. Thus, mean differences are −0.6 Wm^{-2} over Greenland, meaning a slightly greater heat flux under RCP4.5 than G4, while for VIC, G4 has a 10.5 Wm^{-2} higher heat flux than RCP4.5. The significance of the increased heat flux from the ocean is high as can be gauged by comparison with the G4-RCP4.5 differences in radiative forcing (Table 4), where the maximum difference is only 5 Wm^{-2}. The

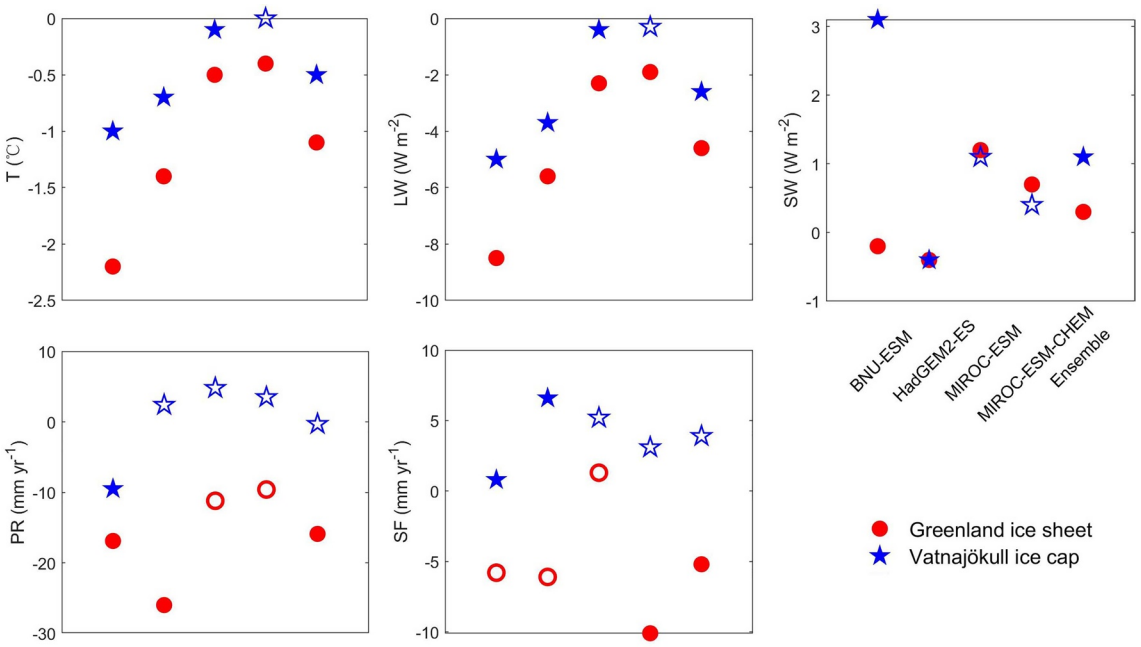

Figure 10. The comparisons of the differences (G4-RCP4.5) of near-surface air temperature (T), downward longwave radiation (LW), downward shortwave radiation (SW), precipitation (PR), and snowfall (SF) over Greenland ice sheet (circle) and Vatnajökull ice cap (star) from four Earth System Models (ESMs) and multimodel mean during the stratospheric aerosol injection (SAI) period 2020–2069. Filled symbols show differences significant at the 95% level with the Wilcoxon signed-rank test.

warmer sea surface around VIC under G4 accounts for the increased precipitation and snowfall (Figure 10) despite globally reduced precipitation and humidity under SAI.

The reason for the relatively increased heat flux around VIC under G4 is that AMOC is more reduced under RCP4.5 than under G4 (Moore et al., 2019). The reduction in AMOC strength leads to reduced heat flux to the overturning regions, especially in the Irminger Basin to the South of Iceland, but also in the Iceland Sea to its north. Figure 12 shows that both mass loss from Greenland and VIC depend on AMOC and how that varies under climate scenarios irrespective of the strength of the response in individual ESMs. During the period 2020–2089, changes in SMB over VIC ($R = 0.64$; $p = 0.03$) is more subject to the AMOC compared to changes over Greenland ($R = 0.51$; $p = 0.09$). Furthermore, the response of SMB to AMOC is even more significant during the 20-year period after termination of SAI than during SAI alone. This is because the AMOC is a relatively slow process due to the large thermal inertia of the ocean and other physical factors, especially sea ice extent, which directly influence AMOC strength.

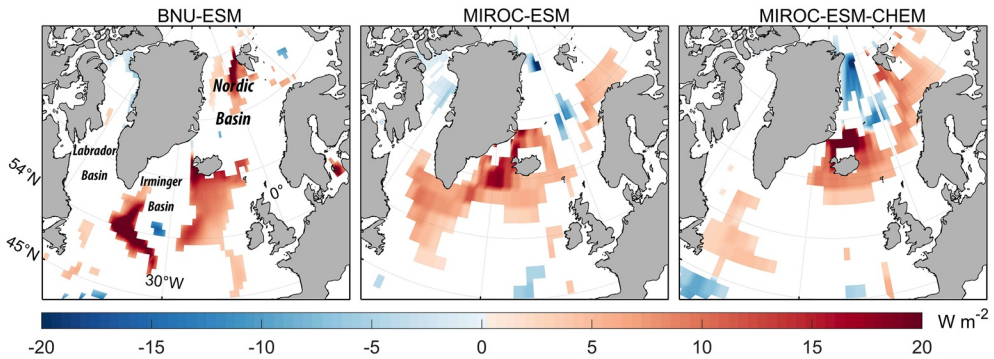

Figure 11. Spatial differences (G4-RCP4.5) of sea surface heat flux from ocean to atmosphere during 2020–2069 modeled by BNU-Earth System Model (ESM) (left), MIROC-ESM (middle), and MIROC-ESM-CHEM (right). Note that we only plot the 95% significant differences through the Wilcoxon sign-rank test. HadGEM2-ES lacks this data.

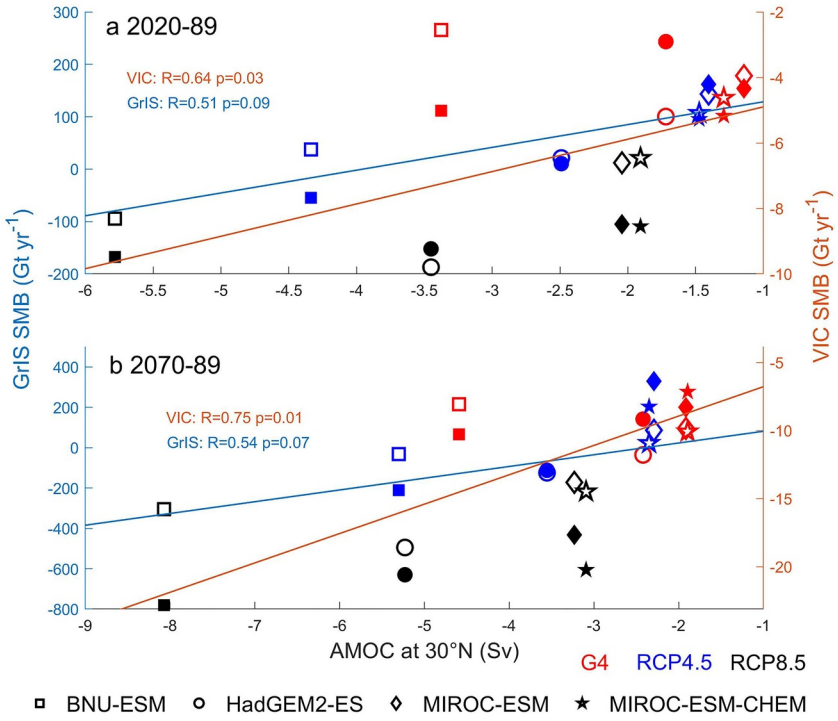

Figure 12. The linear regression analysis between mean surface mass balance (SMB) and Atlantic Meridional Overturning Circulation (AMOC) index anomalies relative to 1990–2005 over Greenland ice sheet (GrIS; unfilled) and Vatnajökull ice cap (VIC) (filled) during the whole period 2020–2089 (a) and only post-stratospheric aerosol injection (SAI) period 2070–2089 under G4 (red), RCP4.5 (blue), and RCP8.5 (black) scenarios from BNU-ESM (square), HadGEM2-ES (circle), MIROC-ESM (diamond), and MIROC-ESM-CHEM (star). The SMB over Greenland are from Moore et al. (2019). The AMOC index is calculated as the annual mean maximum volume transport stream function at 30°N.

4.2. Limitations

This research is the first to explore the VIC response under geoengineering. Using the surface energy and mass balance model SEMIC with bias correction and downscaling to match available remote sensing and surface observation that allows us to use the low-resolution ESM climate output to simulate a relatively small ice cap. Differing from the previous VIC mass balance estimate studies that we mentioned in Section 1, we neglect calving and basal melting under VIC. Basal melting is an important component for total mass balance because of the high geothermal heat flux and active volcanism (Hjartarson, 2015). Jóhannesson et al. (2020) showed this component can amount to ~20%–40% of the magnitude of the SMB over the southern VIC during the period 1995–2019. However, basal melting due to high heat flow is not related to climate, and hence anomalies that show differences caused by climate scenarios would be unaffected. Calving losses from VIC are very limited for all outlets except for Breiðamerkurjökull on the south side of VIC, which calves into the terminal lake Jökulsárlón, where it amounts to about 25% of the losses from basal melting (Jóhannesson et al., 2020). This flux is likely to increase in future as the terminus of several southern outlets retreat into over-deepened basins and are exposed to deeper water. This also impacts the broader issue of our neglecting area change during our simulations. We assume a constant ice area in all simulations, which may therefore overestimate the surface runoff. Schmidt et al. (2020) found that the VIC area will lose 8% and 14% by the year 2089 under RCP4.5 and RCP8.5 scenarios, respectively.

Geoengineering by SAI entails a number of well-studied side effects. The aim of this article has focused on mass balance and the changes in climate over the North Atlantic, but we may mention that SAI simulations show that it would lower ozone concentrations (Pitari et al., 2014), and the aerosols would also absorb radiation, warming the stratosphere and affecting stratospheric chemistry and dynamics (Tilmes et al., 2009). Beyond these, a key issue is that it lacks ethical and governance credibility, and reaching at least near-global consensus is desirable. Instead of modifying the global large-scale climate, a more tractable

approach may be targeted interventions done only regionally to conserve specific elements of the system (Moore et al., 2020; Wolovick & Moore, 2018). One application may be on the high-leverage regions such as ice streams and outlet glaciers (Moore et al., 2018) where melting from oceans dominates potential ice sheet collapse. The limited exposure of Icelandic outlets to oceanic forcing tends to preclude this approach to conserving the ice cap, although the over-deepened basins on the Southern part of VIC might make for engineering test beds of targeted interventions.

Alternatives to the G4 scenario avoiding constant equatorial SO_2 injection into the lower stratosphere have been simulated with very limited numbers of ESMs. The GLENS (Geoengineering Large Ensemble) simulations follow the feedback and control approach designed to maintain temperature gradients against a rising CO_2 background with dynamically adjusted injection rate at four latitudes (Kravitz et al., 2016). A GLENS style implementation of SAI may reduce the side effects caused by SAI such as regional drought and aridity (Irvine & Keith, 2020).

More ESMs with better parameterization of Arctic processes, especially shortwave radiative forcing would help to narrow uncertainties in quantifying mass balance. Furthermore, the detailed response of AMOC overturning is also model dependent, so while the models used here show largest reductions under SAI in the Irminger basin to the South of Iceland, other models show larger changes to the southeast of Greenland and in the Labrador Sea (Liu et al., 2019). It is doubtful that this change in the location of overturning would affect the general conclusion that AMOC is more important for maintaining Icelandic glaciers than for the Greenland ice sheet simply because Iceland as a maritime environment, and VIC is closer to the ocean regions where heat is transferred by AMOC than much of the Greenland ice sheet. In future warming scenarios AMOC is estimated to further weaken, but the degree of weakening still remains largely uncertain, potentially even including an unstable regime that completely collapses as it did in the past (e.g., Rahmstorf, 2002). The AMOC may collapse after the atmospheric CO_2 concentration is doubled from 1990 level, which would lead to a distinct cooling of the northern North Atlantic climates (Liu et al., 2017).

A new generation of ESM is simulating a set of new SAI scenarios, including the new G6sulfer scenario, which is rather similar to G4, but its greenhouse gas background scenario follows the new CMIP6 SSP (Shared Socioeconomic Pathways) scenarios (Kravitz et al., 2015). Few studies have examined the differences of SAI effects in CMIP5 and CMIP6. Existing studies have shown that AMOC decline under future CMIP6 SSP scenarios is much stronger than CMIP5 models, CMIP6 averagely display a 29% and 39% AMOC decline for SSP2-4.5 and SSP5-8.5 scenarios, which are more than the declines of 21% and 36% for RCP4.5 and RCP8.5 scenarios (Cheng et al., 2013; Schleussner et al., 2014; Weijer et al., 2020) The CMIP6 ESMs also show a clear improvement over those in CMIP5 in capturing Arctic climate (e.g., Davy & Outten, 2020).

5. Conclusion

We simulate and project VIC SMB and surface runoff during the period 1982–2089 using the surface energy and mass balance model SEMIC, forced with bias-corrected and downscaled climate outputs from four ESMs.

G4 reduces runoff by 6.2 ± 6% and 7.2 ± 6% compared with RCP4.5 and RCP8.5 over the geoengineering period 2020–2069. The ensemble mean VIC SMB from 2020 to 2069 are −0.34 ± 0.18 m yr^{-1} under G4, -0.56 ± 0.06 m yr^{-1} under RCP4.5, and −0.66 ± 0.04 m yr^{-1} under RCP8.5. The lower runoff and higher SMB under G4 demonstrate the significant cooling effect over the whole VIC, that will continue to hold for at least a decade after the termination of SAI. Thus, SAI could play a role in preserving VIC, but it is notably less effective than it is for the Greenland ice sheet and for High Mountain Asian glaciers. The lack of effectiveness in the VIC response is because of its proximity to the overturning of the AMOC. Greenland was less affected by AMOC changes under SAI than Iceland, and we would therefore expect that glaciers in Alaska and the Siberian Arctic would be the most responsive to solar geoengineering, while those in Svalbard and perhaps Franz Josef Land would be affected to a similar extent as Greenland. The unique location of Iceland means that the amelioration of radiative forcing through solar geoengineering is largely offset by SAI induced maintenance of the strength of the AMOC.

Data Availability Statement

GeoMIP and CMIP5 data are available on the Earth System Grid Federation (https://esgf-node.llnl.gov/). Surface mass balance and surface runoff data modeled by SEMIC are available at http://doi.org/10.5281/zenodo.4922302.

Acknowledgments
This study is supported by the National Key Research and Development Program of China (2018YFC1406104), National Natural Science Foundation of China (No. 41941006), National Basic Research Program of China (2016YFA0602701), Finnish Academy COLD consortium grant 322430. The authors thank two anonymous reviewers made many suggestions to help improving the study.

References

Aðalgeirsdóttir, G., Pálsson, F., Thorsteinsson, T., Magnusson, E., Belart, J., Johannesson, T., et al. (2020). Glacier changes in Iceland from 1890 to 2019. *Frontiers of Earth Science*, *8*. https://doi.org/10.3389/feart.2020.523646

Applegate, P. J., & Keller, K. (2015). How effective is albedo modification (solar radiation management geoengineering) in preventing sea-level rise from the Greenland Ice Sheet? *Environmental Research Letters*, *10*(8), 84018. https://doi.org/10.1088/1748-9326/10/8/084018

Bajat, B., Pejović, M., Luković, J., Manojlović, P., Ducić, V., & Mustafić, S. (2013). Mapping average annual precipitation in Serbia (1961–1990) by using regression kriging. *Theoretical and Applied Climatology*, *112*(1–2), 1–13. https://doi.org/10.1007/s00704-012-0702-2

Björnsson, H., & Pálsson, F. (2008). Icelandic glaciers. *Jökull Journal*, *58*(58), 365–386.

Björnsson, H., Pálsson, F., Gudmundsson, S., Magnússon, E., Adalgeirsdóttir, G., Jóhannesson, T., et al. (2013). Contribution of Icelandic ice caps to sea level rise: Trends and variability since the Little Ice Age. *Geophysical Research Letters*, *40*(8), 1546–1550. https://doi.org/10.1002/grl.50278

Björnsson, H., Pálsson, F., Sigurđsson, O., & Flowers, G. E. (2003). Surges of glaciers in Iceland. *Annals of Glaciology*, *36*, 82–90. https://doi.org/10.3189/172756403781816365

Block, K., Schneider, F. A., Mülmenstädt, J., Salzmann, M., & Quaas, J. (2020). Climate models disagree on the sign of total radiative feedback in the Arctic. *Tellus A: Dynamic Meteorology and Oceanography*, *72*(1), 1–14. https://doi.org/10.1080/16000870.2019.1696139

Bostan, P. A., Heuvelink, G. B. M., & Akyurek, S. Z. (2012). Comparison of regression and kriging techniques for mapping the average annual precipitation of Turkey. *International Journal of Applied Earth Observation and Geoinformation*, *19*, 115–126. https://doi.org/10.1016/j.jag.2012.04.010

Boucher, O, Randall, D, Artaxo, P, Bretherton, C, Feingold, G, Forster, P, et al. (2013). Clouds and aerosols. *Climate change 2013: The physical science basis. Contribution of working group I to the fifth assessment report of the intergovernmental panel on climate change* (pp. 571–658). Cambridge University Press. https://doi.org/10.1017/cbo9781107415324.016

Caesar, L., Rahmstorf, S., Robinson, A., Feulner, G., & Saba, V. (2018). Observed fingerprint of a weakening Atlantic Ocean overturning circulation. *Nature*, *556*(7700), 191–196. https://doi.org/10.1038/s41586-018-0006-5

Chen, Y., Liu, A., & Moore, J. C. (2020). Mitigation of Arctic permafrost carbon loss through stratospheric aerosol geoengineering. *Nature Communications*, *11*(1), 1–10. https://doi.org/10.1038/s41467-020-16357-8

Cheng, W., Chiang, J. C., & Zhang, D. (2013). Atlantic meridional overturning circulation (AMOC) in CMIP5 models: RCP and historical simulations. *Journal of Climate*, *26*(18), 7187–7197. https://doi.org/10.1175/jcli-d-12-00496.1

Collins, W. J., Bellouin, N., Doutriaux-Boucher, M., Gedney, N., Halloran, P., Hinton, T., et al. (2011). Development and evaluation of an Earth-System model: HadGEM2. *Geoscientific Model Development*, *4*(4), 1051–1075. https://doi.org/10.5194/gmdd-4-997-2011

Davy, R., & Outten, S. (2020). The Arctic surface climate in CMIP6: Status and developments since CMIP5[J]. *Journal of Climate*, *33*(18), 8047–8068. https://doi.org/10.1175/jcli-d-19-0990.1

Delhasse, A., Kittel, C., Amory, C., Hofer, S., As, D., van S Fausto, R., & Fettweis, X. (2020). Brief communication: Evaluation of the near-surface climate in ERA5 over the Greenland Ice Sheet. *The Cryosphere*, *14*(3), 957–965. https://doi.org/10.5194/tc-14-957-2020

De Ruyter-de Wildt, M. S., Oerlemans, J., & Björnsson, H. (2004). A calibrated mass balance model for Vatnajökull. *Jökull Journal*, *52*, 1–20.

Farr, T. G., Rosen, P. A., Caro, E., Crippen, R., Duren, R., Hensley, S., et al. (2007). The shuttle radar topography mission. *Reviews of Geophysics*, *45*(2). https://doi.org/10.1029/2005RG000183

Fettweis, X., Franco, B., Tedesco, M., Van Angelen, J. H., Lenaerts, J. T. M., van den Broeke, M. R., & Gallée, H. (2013). Estimating the Greenland ice sheet surface mass balance contribution to future sea level rise using the regional atmospheric climate model MAR. *The Cryosphere*, *7*(2), 469–489. https://doi.org/10.5194/tc-7-469-2013

Flowers, G. E., Marshall, S. J., Björnsson, H., & Clarke, G. K. C. (2005). Sensitivity of Vatnajökull ice cap hydrology and dynamics to climate warming over the next 2 centuries. *Journal of Geophysical Research*, *110*(F2). https://doi.org/10.1029/2004jf000200

Gascoin, S., Guðmundsson, S., Aðalgeirsdóttir, G., Pálsson, F., Schmidt, L., Berthier, E., & Björnsson, H. (2017). Evaluation of MODIS albedo product over ice caps in Iceland and impact of volcanic eruptions on their albedo. *Remote Sensing*, *9*(5), 399. https://doi.org/10.3390/rs9050399

Gong, Y., Zwinger, T., Åström, J., Altena, B., Schellenberger, T., Gladstone, R., & Moore, J. (2018). Simulating the roles of crevasse routing of surface water and basal friction on the surge evolution of Basin 3, Austfonna ice cap. *The Cryosphere*, *12*, 1563–1577. https://doi.org/10.5194/tc-12-1563-2018

Gunnarsson, A., Gardarsson, S. M., Pálsson, F., Jóhannesson, T., & Sveinsson, Ó. G. B. (2021). Annual and inter-annual variability and trends of albedo of Icelandic glaciers. *The Cryosphere*, *15*(2), 547–570. https://doi.org/10.5194/tc-15-547-2021

Guðmundsson, S., Björnsson, H., Magnússon, E., Berthier, E., Pálsson, F., Gudmundsson, M. T., et al. (2011). Response of Eyjafjallajökull, Torfajökull and Tindfjallajökull ice caps in Iceland to regional warming, deduced by remote sensing. *Polar Research*, *30*(1), 7282. https://doi.org/10.3402/polar.v30i0.7282

Guðmundsson, S., Björnsson, H., Pálsson, F., & Haraldsson, H. H. (2009). Comparison of energy balance and degree-day models of summer ablation on the Langjökull ice cap, SW-Iceland. *Jökull Journal*, *59*, 1–18.

Hassan, T., Allen, R. J., Liu, W., & Randles, C. A. (2021). Anthropogenic aerosol forcing of the Atlantic meridional overturning circulation and the associated mechanisms in CMIP6 models. *Atmospheric Chemistry and Physics*, *21*(8), 5821–5846. https://doi.org/10.5194/acp-21-5821-2021

Hempel, S., Frieler, K., Warszawski, L., Schewe, J., & Piontek, F. (2013). A trend-preserving bias correction: The ISI-MIP approach. *Earth System Dynamics*, *4*(2), 219–236. https://doi.org/10.5194/esd-4-219-2013

Hersbach, H., Bell, B., Berrisford, P., Hirahara, S., Horányi, A., Muñoz-Sabater, J., et al. (2020). The ERA5 global reanalysis. *Quarterly Journal of the Royal Meteorological Society*, *146*(730), 1999–2049. https://doi.org/10.1002/qj.3803

Hjartarson, Á. (2015). Heat flow in Iceland. *Proceedings world geothermal congress*.

Hong, Y., Moore, J. C., Jevrejeva, S., Ji, D., Phipps, S. J., Lenton, A., et al. (2017). Impact of the GeoMIP G1 sunshade geoengineering experiment on the Atlantic meridional overturning circulation. *Environmental Research Letters*, *12*(3), 34009. https://doi.org/10.1088/1748-9326/aa5fb8

Irvine, P. J., & Keith, D. W. (2020). Halving warming with stratospheric aerosol geoengineering moderates policy-relevant climate hazards. *Environmental Research Letters*, *15*(4), 44011. https://doi.org/10.1088/1748-9326/ab76de

Irvine, P. J., Keith, D. W., & Moore, J. (2018). Brief communication: Understanding solar geoengineering's potential to limit sea level rise requires attention from cryosphere experts. *The Cryosphere*, *12*(7), 2501–2513. https://doi.org/10.5194/tc-12-2501-2018

Irvine, P. J., Lunt, D. J., Stone, E. J., & Ridgwell, A. (2009). The fate of the Greenland Ice Sheet in a geoengineered, high CO_2 world. *Environmental Research Letters*, *4*(4), 45109. https://doi.org/10.1088/1748-9326/4/4/045109

Ji, D., Wang, L., Feng, J., Wu, Q., Cheng, H., Zhang, Q., et al. (2014). Description and basic evaluation of Beijing Normal University Earth system model (BNU-ESM) version 1. *Geoscientific Model Development*, *7*(5), 2039–2064. https://doi.org/10.5194/gmd-7-2039-2014

Jóhannesson, T., Pálmason, B., Hjartarson, Á., Jarosch, A. H., Magnússon, E., Belart, J. M. C., & Gudmundsson, M. T. (2020). Non-surface mass balance of glaciers in Iceland. *Journal of Glaciology*, *66*(258), 685–697. https://doi.org/10.1017/jog.2020.37

Kipp, Z., & Zonen, B. V. (2000). *CNR1 net radiometer instruction manual*. Kipp & Zonen, Delft.

Kitous, A., & Keramidas, K. (2015). *Analysis of scenarios integrating the INDCs*. European Comission.

Krapp, M., Robinson, A. J., & Ganopolski, A. (2017). SEMIC: An efficient surface energy and mass balance model applied to the Greenland ice sheet. *The Cryosphere*, *11*(4), 1519–1535. https://doi.org/10.5194/tc-11-1519-2017

Kravitz, B., Caldeira, K., Boucher, O., Robock, A., Rasch, P. J., Alterskjaer, K., et al. (2013). Climate model response from the Geoengineering Model Intercomparison Project (GeoMIP). *Journal of Geophysical Research: Atmospheres*, *118*, 8320–8332. https://doi.org/10.1002/jgrd.50646

Kravitz, B., MacMartin, D. G., Wang, H., & Rasch, P. J. (2016). Geoengineering as a design problem. *Earth System Dynamics*, *7*, 469–497. https://doi.org/10.5194/esd-7-469-2016

Kravitz, B., Robock, A., Tilmes, S., Boucher, O., English, J. M., Irvine, P. J., et al. (2015). The geoengineering model intercomparison project phase 6 (GeoMIP6): Simulation design and preliminary results[J]. *Geoscientific Model Development*, *8*(10), 3379–3392. https://doi.org/10.5194/gmd-8-3379-2015

Lee, W. R., MacMartin, D. G., Visioni, D., & Kravitz, B. (2021). High-latitude stratospheric aerosol geoengineering can be more effective if injection is limited to spring. *Geophysical Research Letters*, *48*, e2021GL092696. https://doi.org/10.1029/2021GL092696

Liang, S., Zhao, X., Liu, S., Yuan, W., Cheng, X., Xiao, Z., et al. (2013). A long-term Global LAnd Surface Satellite (GLASS) data-set for environmental studies. *International Journal of Digital Earth*, *6*, 5–33. https://doi.org/10.1080/17538947.2013.805262

Liu, W., Fedorov, A., & Sévellec, F. (2019). The mechanisms of the Atlantic meridional overturning circulation slowdown induced by Arctic sea ice decline. *Journal of Climate*, *32*(4), 977–996. https://doi.org/10.1175/JCLI-D-18-0231.1

Liu, W., Xie, S.-P., Liu, Z., & Zhu, J. (2017). Overlooked possibility of a collapsed Atlantic Meridional Overturning Circulation in warming climate. *Science Advances*, *3*(1), e1601666. https://doi.org/10.1126/sciadv.1601666

Ma, X., Liu, W., Allen, R. J., Huang, G., & Li, X. (2020). Dependence of regional ocean heat uptake on anthropogenic warming scenarios. *Science Advances*, *6*(45), eabc0303. https://doi.org/10.1126/sciadv.abc0303

Marshall, S. J., Björnsson, H., Flowers, G. E., & Clarke, G. K. C. (2005). Simulation of Vatnajökull ice cap dynamics. *Journal of Geophysical Research*, *110*(F3). https://doi.org/10.1029/2004jf000262

Menary, M. B., Robson, J., Allan, R. P., Booth, B. B. B., Cassou, C., Gastineau, G., et al. (2020). Aerosol-forced AMOC changes in CMIP6 historical simulations. *Geophysical Research Letters*, *47*(14), e2020GL088166. https://doi.org/10.1029/2020GL088166

Moore, J. C., Gladstone, R., Zwinger, T., & Wolovick, M. (2018). Geoengineer polar glaciers to slow sea-level rise. *Nature*, *555*, 303–305. https://doi.org/10.1038/d41586-018-03036-4

Moore, J. C., Mettiäinen, I., Wolovick, M., Zhao, L., Gladstone, R., Chen, Y., et al. (2020). Targeted Geoengineering: Local Interventions with Global Implications. *Global Policy*, *12*, 108–118. https://doi.org/10.1111/1758-5899.12867

Moore, J. C., Yue, C., Zhao, L., Guo, X., Watanabe, S., & Ji, D. (2019). Greenland ice sheet response to stratospheric aerosol injection geoengineering. *Earth's Future*, *7*(12), 1451–1463. https://doi.org/10.1029/2019ef001393

Mouginot, J., Rignot, E., Bjørk, A. A., van den Broeke, M., Millan, R., Morlighem, M., et al. (2019). Forty-six years of Greenland Ice Sheet mass balance from 1972 to 2018. *Proceedings of the National Academy of Sciences of the USA*, *116*(19), 9239–9244. https://doi.org/10.1073/pnas.1904242116

Ólafsson, H., Furger, M., & Brümmer, B. (2007). The weather and climate of Iceland. *Meteorologische Zeitschrift*, *16*(1), 5–8. https://doi.org/10.1127/0941-2948/2007/0185

Pálsson, F., Gunnarsson, A., Jónsson, G., Pálsson, H. S., & Steinþórsson, S. (2017). *Vatnajökull: Mass balance, meltwater drainage and surface velocity of the glacial year 2016_17*. Institute of Earth Sciences, University of Iceland and National Power Company.

Pálsson, F., Gunnarsson, A., Jónsson, Þ., Steinþórsson, S., & Pálsson, H. S. (2015). *Vatnajökull: Mass balance, meltwater drainage and surface velocity of the glacial year 2014_15*. Institute of Earth Sciences, University of Iceland and National Power Company.

Pitari, G., Aquila, V., Kravitz, B., Robock, A., Watanabe, S., Cionni, I., et al. (2014). Stratospheric ozone response to sulfate geoengineering: Results from the Geoengineering Model Intercomparison Project (GeoMIP). *Journal of Geophysical Research: Atmospheres*, *119*(5), 2629–2653. https://doi.org/10.1002/2013jd020566

Rahmstorf, S. (2002). Ocean circulation and climate during the past 120,000 years. *Nature*, *419*(6903), 207–214. https://doi.org/10.1038/nature01090

Rahmstorf, S., Box, J. E., Feulner, G., Mann, M. E., Robinson, A., Rutherford, S., & Schaffernicht, E. J. (2015). Exceptional twentieth-century slowdown in Atlantic Ocean overturning circulation. *Nature Climate Change*, *5*(5), 475–480. https://doi.org/10.1038/nclimate2554

Renfrew, I. A., Barrell, C., Elvidge, A. D., Brooke, J. K., Duscha, C., King, J. C., et al. (2020). An evaluation of surface meteorology and fluxes over the Iceland and Greenland Seas in ERA5 reanalysis: The impact of sea ice distribution. *Quarterly Journal of the Royal Meteorological Society*, *147*, 691–712. https://doi.org/10.1002/qj.3941

Riahi, K., Rao, S., Krey, V., Cho, C., Chirkov, V., Fischer, G., et al. (2011). RCP 8.5: A scenario of comparatively high greenhouse gas emissions. *Climatic Change*, *109*(1–2), 33–57. https://doi.org/10.1007/s10584-011-0149-y

Robson, J., Hodson, D., Hawkins, E. D., & Sutton, R. (2014). Atlantic overturning in decline? *Nature Geoscience*, *7*(1), 2–3. https://doi.org/10.1038/ngeo2050

Rückamp, M., Falk, U., Frieler, K., Lange, S., & Humbert, A. (2018). The effect of overshooting 1.5°C global warming on the mass loss of the Greenland ice sheet. *Earth System Dynamics*, *9*(4), 1169–1189. https://doi.org/10.5194/esd-9-1169-2018

Schleussner, C. F., Levermann, A., & Meinshausen, M. (2014). Probabilistic projections of the Atlantic overturning. *Climatic Change*, *127*(3–4), 579–586. https://doi.org/10.1007/s10584-014-1265-2

Schmidt, L. S., Aðalgeirsdóttir, G., Guðmundsson, S., Langen, P. L., Pálsson, F., Mottram, R., et al. (2017). The importance of accurate glacier albedo for estimates of surface mass balance on Vatnajökull: Evaluating the surface energy budget in a regional climate model with automatic weather station observations. *The Cryosphere*, *11*, 1665–1684. https://doi.org/10.5194/tc-11-1665-20110.5194/tc-11-1665-2017

Schmidt, L. S., Aðalgeirsdóttir, G., Pálsson, F., Langen, P. L., Guðmundsson, S., & Björnsson, H. (2020). Dynamic simulations of Vatnajökull ice cap from 1980 to 2300. *Journal of Glaciology*, *66*(255), 97–112. https://doi.org/10.1017/jog.2019.90

Schmidt, L. S., Langen, P. L., Aðalgeirsdóttir, G., Pálsson, F., Guðmundsson, S., & Gunnarsson, A. (2018). Sensitivity of glacier runoff to winter snow thickness investigated for Vatnajökull ice cap, Iceland, using numerical models and observations. *Atmosphere*, *9*(11), 450. https://doi.org/10.3390/atmos9110450

Shepherd, J. G. (2009). *Geoengineering the climate: Science, governance and uncertainty*. Royal Society.

Smith, W., & Wagner, G. (2018). Stratospheric aerosol injection tactics and costs in the first 15 years of deployment. *Environmental Research Letters*, *13*(12), 124001. https://doi.org/10.1088/1748-9326/aae98d

Thomson, A. M., Calvin, K. V., Smith, S. J., Kyle, G. P., Volke, A., Patel, P., et al. (2011). RCP4. 5: A pathway for stabilization of radiative forcing by 2100. *Climatic Change*, *109*(1–2), 77–94. https://doi.org/10.1007/s10584-011-0151-4

Tilmes, S., Garcia, R. R., Kinnison, D. E., Gettelman, A., & Rasch, P. J. (2009). Impact of geoengineered aerosols on the troposphere and stratosphere. *Journal of Geophysical Research*, *114*(D12). https://doi.org/10.1029/2008jd011420

Tilmes, S., MacMartin, D. G., Lenaerts, J. T. M., van Kampenhout, L., Muntjewerf, L., Xia, L., et al. (2020). Reaching 1.5 and 2.0 °C global surface temperature targets using stratospheric aerosol geoengineering. *Earth System Dynamics*, *11*, 579–601. https://doi.org/10.5194/esd-11-579-2020

Vilhjálmsson, H. (2002). Capelin (Mallotus villosus) in the Iceland–East Greenland–Jan Mayen ecosystem. *ICES Journal of Marine Science*, *59*(5), 870–883. https://doi.org/10.1006/jmsc.2002.1233

Watanabe, S., Hajima, T., Sudo, K., Nagashima, T., Takemura, T., Okajima, H., et al. (2011). MIROC-ESM 2010: Model description and basic results of CMIP5-20c3m experiments. *Geoscientific Model Development*, *4*(4), 845–872. https://doi.org/10.5194/gmd-4-845-2011

Weijer, W., Cheng, W., Garuba, O. A., Hu, A., Nadiga, B. T., et al. (2020). CMIP6 models predict significant 21st century decline of the Atlantic Meridional Overturning Circulation[J]. *Geophysical Research Letters*, *47*(12), e2019GL086075. https://doi.org/10.1029/2019gl086075

Wild, M., Folini, D., Schär, C., Loeb, N., Dutton, E., & König-Langlo, G. (2013). The global energy balance from a surface perspective. *Climate Dynamics*, *40*, 3107–3134. https://doi.org/10.1007/s00382-012-1569-8

Wittmann, M., Groot Zwaaftink, C. D., Steffensen Schmidt, L., Guðmundsson, S., Pálsson, F., Arnalds, O., et al. (2017). Impact of dust deposition on the albedo of Vatnajökull ice cap, Iceland. *The Cryosphere*, *11*(2), 741–754. https://doi.org/10.5194/tc-2016-205-rc210.5194/tc-11-741-2017

Wolovick, M. J., & Moore, J. C. (2018). Stopping the flood: Could we use targeted geoengineering to mitigate sea level rise? *The Cryosphere*, *12*(9), 2955–2967. https://doi.org/10.5194/tc-12-2955-2018

Zhao, L., Yang, Y., Cheng, W., Ji, D., & Moore, J. C. (2017). Glacier evolution in high-mountain Asia under stratospheric sulfate aerosol injection geoengineering. *Atmospheric Chemistry and Physics*, *17*(11), 6547–6564. https://doi.org/10.5194/acp-17-6547-2017

Reference From the Supporting Information

Slater, A. G., Pitman, A. J., & Desborough, C. E. (1998). The validation of a snow parameterization designed for use in general circulation models. *International Journal of Climatology: A Journal of the Royal Meteorological Society*, *18*(6), 595–617. https://doi.org/10.1002/(SICI)1097-0088(199805)18:6%3C595::AID-JOC275%3E3.0.CO;2-O